



Fermi National Accelerator Laboratory

FERMILAB-Conf-89/207-E
[E-741/CDF]

Recent Results from the CDF Experiment at the Tevatron Proton-Antiproton Collider *

The CDF Collaboration

presented by

S. Geer
Harvard University
High Energy Physics Laboratory
42 Oxford St.,
Cambridge, MA 02138

September 1989

* Presented at the 8th INFN Eloisatron Project Workshop on the Higgs Boson, Erice, Italy, July 15-26, 1989.



Recent Results from the CDF Experiment at the Tevatron Proton-Antiproton Collider

The CDF Collaboration
presented by

S. Geer

Harvard University,
High Energy Physics Laboratory,
42 Oxford Street, Cambridge MA 02138

Abstract

Recent results from the CDF experiment are described. The Standard Model gives a good description of jet production, and W/Z production and decay. There is no evidence yet for the top quark, for fourth generation quarks, or for deviations from the Standard Model ascribable to quark substructure, supersymmetric particles, or heavy additional W-like or Z-like bosons. Limits are given where applicable. A search for a light Higgs Boson is also described.

Presented at the 8th INFN Eloisatron Project Workshop on the Higgs Boson,
Erice, Italy, July 1989.

1. Introduction

The Collider Detector at Fermilab (CDF) had its first physics run in 1987 and recorded 25 nb^{-1} of proton-antiproton collisions at a centre-of-mass energy of 1.8 TeV at the Tevatron collider. In 1988 CDF began a second highly successful physics run which ended in June 1989, and recorded a total integrated luminosity of 4.7 pb^{-1} . In the following sections physics results are reported from both the 1987 and 1988/9 runs. The topics covered include hadronic jet production and fragmentation, W and Z production and decay, the search for supersymmetric particles, the top quark, and the Higgs boson.

1.1 The CDF Detector

The CDF detector is a 5000 t magnetic detector. A side view of the detector is shown in fig. 1. Event analysis is based on charged particle tracking, magnetic momentum analysis, and fine-grained calorimetry. The combined electromagnetic and hadron calorimetry has approximately uniform granularity in pseudorapidity (η) - azimuthal angle (ϕ) space, and extends down to 2° from the beam directions. Various tracking chambers cover the calorimeter acceptance and extend charged particle tracking down to 2 mrad from the beam directions. Charged particle momenta are analyzed in a 1.5T solenoidal magnetic field, generated by a superconducting coil which is 3 m in diameter and 5 m in length. The central tracking chamber (CTC) measures particle momenta with a resolution better than $\delta p_T/p_T^2 = 0.002 \text{ (GeV/c)}^{-1}$ in the region $40^\circ < \theta < 140^\circ$ and $\delta p_T/p_T^2 \leq 0.004 \text{ (GeV/c)}^{-1}$ for $21^\circ < \theta < 40^\circ$ and $140 < \theta < 159^\circ$. The calorimeters, which have full azimuthal angle coverage, consist of electromagnetic (EM) shower counters and hadron calorimeters, and are segmented into about 5000 projective towers. Each tower is 0.1 units of η wide by 15° in ϕ in the central region ($|\eta| < 1.1$) and 5° in ϕ elsewhere. Muon coverage is provided by drift chambers in the region $56^\circ < \theta < 124^\circ$, and by large forward toroid systems in the range $3^\circ < \theta < 16^\circ$ and $164^\circ < \theta < 177^\circ$. Isolated high momentum muons can be identified in the intermediate angular range in many cases by a comparison of the tracking and calorimeter information. Custom-built front-end electronics followed by a large Fastbus network provides the readout of approximately 100 000 detector channels. Fast level 1 and level 2 triggers make a detailed pre-analysis of calorimeter and tracking information. A level 3 trigger system uses on-line processors to perform parallel event processing. A more detailed description of the detector can be found in ref. [1].

2. Jet Physics

Jets are reconstructed in CDF using a cone algorithm which clusters the energy around a central seed calorimeter tower (transverse energy $E_T > 1$ GeV) in a cone in (η, ϕ) -space with radius $\Delta R \equiv \sqrt{\Delta\eta^2 + \Delta\phi^2} = 0.7$. The cluster direction is then calculated and any additional towers within a cone $\Delta R = 0.7$ around the cluster direction added to the cluster. This process is repeated until no new towers are added to the cluster. To obtain the energy of the underlying parton the cluster energies are corrected for non-linear calorimeter response to low energy pions, leakage, uninstrumented regions of the detector, and the contribution from the underlying spectator event. The energy corrections depend on the jet transverse energy, and are 33% for jets with E_T of 20 GeV, decreasing to 17% for jets with E_T of 400 GeV. The uncertainty on these corrections is 12% at 20 GeV and 4% at 400 GeV. The dominant source of the uncertainty comes from the lack of knowledge of the jet fragmentation function combined with the non-linearity of the calorimeter response. Further details of the jet reconstruction method and jet energy corrections can be found in ref. [2].

2.1 The Inclusive Jet Cross-Section

To ensure good containment in the central calorimeter, jets have been analysed if the jet axis is within the region $0.1 < |\eta| < 0.7$, and the event vertex co-ordinate along the beam direction is within 60 cm of the center of the detector. To eliminate background from cosmic rays and beam halo, events with a significant amount of energy not in time with the beam crossing were eliminated. To further reject backgrounds, jets with $E_T > 80$ GeV were required to deposit at least 10% and not more than 95% of their energy in the EM calorimeter, and the missing E_T in the event was required to be small ($< 4.8\sqrt{E_T} \sim 6\sigma$). These cuts are estimated to reject $> 99\%$ of the background, retaining $> 97\%$ of the true jet cross-section.

A preliminary measurement of the inclusive differential jet cross-section per unit of rapidity in the central region is shown in fig. 2 based on 1.4 pb^{-1} of 1988/9 data. The differential cross-section has been corrected for the experimental energy resolution, which can be parameterized by

$$\frac{\sigma(E_{\text{JET}})}{E_{\text{JET}}} = \frac{110\%}{\sqrt{E_{\text{JET}}}}.$$

The smearing correction increases the measured cross-section by 70% at the lowest measured jet energies, and 12% at the highest energies. The uncertainties shown on the measurements are a combination of statistical and E_T dependent systematic errors. In addition there is an E_T independent systematic error arising from uncertainties in the integrated luminosity (15%), smearing correction (10%), and jet energy scale (50%). The normalization uncertainty is indicated on the figure. The inclusive differential jet cross-section is well described by the lowest order prediction evaluated at $Q^2 = E_T^2/2$ using the structure functions of Duke and Owens set 2 [3]. There is no hint of a flattening of the jet E_T distribution at high E_T due to quark substructure [4].

2.2 Two-jet Angular- and Mass-Distributions

To obtain the two-jet angular distribution a preliminary analysis has been made of 800 nb⁻¹ of 1988/9 data, requiring at least one jet with uncorrected $E_T > 80$ GeV and pseudorapidity $|\eta| < 0.7$ that is coplanar ($\pm 30^\circ$) with a second jet. The jets are treated as massless objects, and their pseudorapidities η_1 and η_2 determined from the centroids of the associated clusters. Defining

$$\eta^* \equiv \frac{(\eta_1 - \eta_2)}{2}$$

we require $|\eta^*| < 1.0$. The center-of-mass momentum

$$p^* \equiv p_T \cosh(\eta^*)$$

is required to be in excess of 150 GeV/c so that the angular distribution is unbiased by the η^* cut. The center-of-mass angular variable $\cos \theta^*$ is given by

$$\cos \theta^* = \tanh(\eta^*) .$$

Fig. 3 shows a preliminary measurement of the resulting two-jet angular distribution $dN/d\cos\theta^*$. The distribution has not been corrected for acceptance, however these corrections are expected to be less than 15%. As expected the measured distribution is similar to the predicted leading order QCD prediction.

A preliminary measurement of the two-jet mass distribution based on the full 1988/9 statistics (4.7 pb⁻¹) is shown in fig. 4. The distribution extends to masses of ~ 800 GeV/c², and is well described by leading order QCD expectations.

2.3 Jet Fragmentation

Jet fragmentation has been studied using two-jet data from the 1987 run. Events were selected with two leading jets which were coplanar ($\pm 30^\circ$), and for which there were no other large clusters ($E_T < 20$ GeV or $0.2 (E_T^1 + E_T^2)$, whichever is smaller) in the event. The jets were required to be contained within the central calorimeter ($0.1 < |\eta| < 0.7$), and the boost variable $\eta_{\text{boost}} \equiv 0.5 [\eta_1 + \eta_2]$ was required to be small ($|\eta_{\text{boost}}| < 0.6$). Events were boosted along the beam axis by η_{boost} and well measured charged tracks associated to the primary vertex were associated to a jet if they fell within a cone of opening angle 48° around the jet axis and if their projected momentum along the jet axis $p_{//} > 0.6$ GeV/c. The measured charged fragmentation function

$$D(z) \equiv \frac{1}{N_{\text{jet}}} \frac{dN_{\text{charged}}}{dz}$$

is shown in fig. 5, where the fragmentation variable $z \equiv p_{//} / E_{\text{jet}}$. The track reconstruction efficiency has been estimated as a function of z and two-jet mass using a Monte Carlo, and corrected for. The reconstruction efficiency exceeds 85% for moderate two-jet masses (< 200 GeV/c²). Corrections have also been applied for tracks outside of the CTC acceptance or the jet reconstruction cone, and for the contribution within the cone from uncorrelated tracks from the underlying spectator event. These corrections are only significant at small z . Finally $D(z)$ has been corrected for the experimental resolution on the measurement of E_{jet} and $p_{//}$. The resulting $D(z)$ is similar to the corresponding measurement of jets produced in proton-antiproton collisions at $\sqrt{s} = 630$ GeV by the UA1 collaboration [5]. The variation of $D(z)$ with z and two-jet mass is shown in fig. 6, where it is compared with e^+e^- data from the TASSO experiment [6]. Both experiments show the same trend : namely that the fragmentation becomes more peaked at low z as the four-momentum-transfer squared (Q^2) increases. Fits to the two data sets are of the form expected as a result of the Altarelli-Parisi evolution : $D(z, m_{jj}) = \alpha + \beta \log(m_{jj})$. It should be noted that the TASSO jets are typically quark jets, whereas the CDF jets in this m_{jj} range are predominantly gluon jets.

3. W and Z Physics

The production and decay properties of the charged (W) and neutral (Z) Intermediate Vector Bosons provide us with an excellent test of both the electroweak and

QCD sectors of the standard model. The CDF experiment has observed the decay modes $W \rightarrow e\nu$, $W \rightarrow \mu\nu$, $Z \rightarrow e^+e^-$, and $Z \rightarrow \mu^+\mu^-$. Work is also in progress on the tau-lepton decay modes of the W and Z.

3.1 W Mass

A preliminary measurement of the W mass has been made using 4.7 pb^{-1} of 1988/9 data. Electron-neutrino decays of the W were selected by requiring an energetic EM cluster ($E_T > 25 \text{ GeV}$) produced in association with a large significant missing transverse energy ($\Delta E_T > 25 \text{ GeV}$, $\Delta E_T/\sqrt{\Sigma E_T} > 2.4$). The calorimeter cluster was further required to have at least 85% of its energy in the EM calorimeter, and an associated charged track such that $E/P < 1.4$. To obtain a clean well measured sample of W decays, events were rejected if there were any additional clusters ($E_T > 7 \text{ GeV}$) in the event, and the electron was required to be central ($|\eta| < 1.0$). Since the longitudinal component of the neutrino momentum is not measured in the CDF detector, the invariant mass of the electron-neutrino system cannot be reconstructed directly. Instead the electron neutrino transverse mass

$$m_T^{e\nu} \equiv \sqrt{2E_T^e E_T^\nu (1 - \cos\phi_{e\nu})}$$

is used, where E_T^ν is identified with the missing transverse energy in the event. The $m_T^{e\nu}$ distribution for the selected W sample is shown in fig. 7. To extract the W mass m_W this distribution has been fitted using a Monte Carlo calculation to model the expected shape of the distribution as a function of m_W . The Monte Carlo includes the distortion of the $m_T^{e\nu}$ distribution due to the finite transverse momentum of the W (P_T^W) and due to the calorimeter resolution. Allowing both the W mass and width to vary the resulting best fit (fig. 7) gives a good description of the data, and yields a preliminary result for the W mass of $m_W = 80.0 \pm 0.2 \text{ (stat)} \pm 0.3 \text{ (scale)} \pm 0.5 \text{ (sys)} \text{ GeV}/c^2$. The main systematic uncertainties arise from the uncertainty in modelling the P_T^W distribution, the ΔE_T resolution ($\delta m_W \sim 400 \text{ MeV}/c^2$), and the uncertainty on the structure function ($\delta m_W \sim 300 \text{ MeV}/c^2$).

3.2 Z Mass

CDF has measured the mass of the Z using $Z \rightarrow \mu^+\mu^-$ tracking data and $Z \rightarrow e^+e^-$ calorimeter data. Results are based on an integrated luminosity of 4.7 pb^{-1} . The analyses are restricted to the central region to exploit the optimum track momentum and calorimeter energy resolutions.

Dimuon events were selected by requiring (1) two tracks with $P_T > 20$ GeV/c; (2) at least one match in ϕ between a muon chamber track segment and a CTC track; (3) non-zero hadronic and EM energy deposition; but less than 6 GeV and 2 GeV respectively in a single calorimeter tower associated with each track; (4) no jets with $E_T > 15$ GeV within 10° of these tracks. Events with two muons back to back ($\Delta\eta = \pm 0.1$, $\Delta\phi = \pm 1.5^\circ$) were rejected as cosmic rays. Events having muon pairs with invariant masses between 50 and 150 GeV/c² were selected (132 events).

Transverse momenta are calculated from track curvature in the 1.4116 Tesla magnetic field, known to $\pm 0.05\%$. The CTC alignment was adjusted using electrons from W decay so that the ratio of track momentum to calorimeter energy was charge independent. The alignment was checked using cosmic ray muons. The CTC alignment and the magnitude of the magnetic field were verified by studying $K_s^0 \rightarrow \pi^+\pi^-$, J/ψ (fig. 8b) and $Y(1S) \rightarrow \mu^+\mu^-$ (fig. 8a) decays. The tracks were constrained to come from the beam axis (beam constraint) in the latter two data samples. The reconstructed masses of 0.498 ± 0.002 , 3.097 ± 0.001 , and 9.469 ± 0.010 GeV/c² agree well with world-average values. Based on these measurements we estimate a mass error $< 0.2\%$ due to systematic momentum scale uncertainties. The beam constraint has been applied to the lepton tracks in the Z data samples. The momentum resolution after applying this constraint is $\delta P_T/P_T^2 = 0.0011$ (GeV/c)⁻¹. Radiative corrections (internal and external bremsstrahlung) were studied using a Monte Carlo event generator which used the exact matrix elements to order α^2 [7] and a detailed simulation of the CDF detector.

The mass distribution for $Z \rightarrow \mu^+\mu^-$ (fig. 9a) was fitted using a maximum likelihood fit with a signal modeled by a relativistic Breit-Wigner convoluted with a Gaussian resolution in $1/P_T$. The fitted mass and width are 90.7 ± 0.4 (stat) ± 0.2 (scale) GeV/c² and 4.0 ± 1.2 (stat) ± 1.0 (syst) GeV. The fit is insensitive to the non-resonant Drell-Yan contribution. The effects of radiative corrections, different structure functions, and the mass window used are included in the estimate of the uncertainties (Table 1).

An inclusive electron sample was obtained by requiring at least one electron candidate satisfying the following: (1) the electron is away from calorimeter tower edges; (2) a ratio of hadronic to EM calorimeter energy of < 0.1 ; (3) a ratio of EM energy to track momentum $E/P < 1.4$; (4) a transverse shower profile in the strip chambers consistent with an electron shower; (5) a match between the strip chamber shower position and the extrapolated track position. A sample of 73 events have electron pairs with both particles satisfying the above criteria and with invariant mass between 50 and 150 GeV/c². The

previously described mass fitting technique using track information was applied to the $Z \rightarrow e^+e^-$ event sample (fig. 9b and Table 1). The radiative effects on the observed mass are appreciably larger than in the muon mode; consequently the best measurement of the Z mass in this mode is obtained using calorimeter information. To determine the Z mass from the calorimeter, the EM calorimeter was calibrated on a tower-by-tower basis using the fitted means of the E/P distributions from a sample of ~ 17000 inclusive electrons. The measured energy resolution of the calorimeter for EM showers is

$$\left(\frac{\sigma_E}{E}\right)^2 = \left(\frac{13.5\%}{\sqrt{E \sin\theta}}\right)^2 + (1.7\%)^2$$

where the constant term arises from the average uncertainty in the individual tower calibrations. The overall energy scale was established from the momentum scale using the mean E/P from ~ 1000 W decay electrons. The expected shape and mean of the E/P distribution for these W electrons was simulated including external and small angle internal bremsstrahlung (fig. 10). For $E/P < 1.4$ the mean E/P is 1.026. The systematic uncertainty in E/P is estimated to be $\pm 0.4\%$. The E/P distribution for Z decay electrons is consistent with the predictions. A small correction was applied to the Z mass for internal wide-angle photon emission (Table 1).

Table 1 : Summary of Z mass measurement corrections and results.

	$Z \rightarrow \mu^+\mu^-$ (tracking)	$Z \rightarrow e^+e^-$ (tracking)	$Z \rightarrow e^+e^-$ (Calorimeter)
# events used in fit	123	58	65
Observed Fitted Mass	90.41 ± 0.40	89.27 ± 0.80	90.93 ± 0.34
Radiative Corrections	$+0.22 \pm 0.03$	$+2.19 \pm 0.30$	$+0.11 \pm 0.03$
Structure Functions	$+0.08 \pm 0.03$	$+0.08 \pm 0.03$	$+0.08 \pm 0.03$
E/P Calibration			± 0.20
Mass Scale	± 0.20	± 0.20	± 0.20
Corrected Mass	$90.7 \pm 0.4 \pm 0.2$	$91.5 \pm 0.8 \pm 0.4$	$91.1 \pm 0.3 \pm 0.4$

The mass and width of the Z peak (fig. 11) were fitted using the maximum likelihood method. The corrected fitted values for the Z mass and width are $91.1 \pm 0.3 \pm 0.4$ GeV/c² and $3.6 \pm 1.1 \pm 1.0$ GeV respectively. The quoted systematic uncertainties reflect reasonable variations in the energy resolution, mass window, choice of structure functions, and fitting procedure.

The corrections and uncertainties in each of the mass measurements are summarized in Table 1. Our best value for the Z mass is a weighted mean of the tracking measurement of the $\mu^+\mu^-$ sample and the calorimeter measurement of the e^+e^- sample. The resulting Z mass is 90.9 ± 0.3 (stat+sys) ± 0.2 (scale) GeV/c² and the width is $3.8 \pm 0.8 \pm 1.0$ GeV. Further details of this analysis can be found in ref. [8].

3.3 Standard Model Parameters

Defining

$$\sin^2 \theta_W \equiv 1 - \left(\frac{m_W}{m_Z} \right)^2$$

and using the measured m_W and m_Z obtained from the electron channels, we obtain $\sin^2 \theta_W = 0.229 \pm 0.012$, which is in excellent agreement with the world average value of 0.230 ± 0.005 (fig. 12a). Due to radiative corrections the W and Z masses also depend upon the top quark mass and, to a lesser extent, the Higgs boson mass. The dependence is shown in fig. 12b.

3.4 Search for Heavy Ws and Zs

No high-mass peaks have been observed by CDF in the $e\nu$ or e^+e^- mass spectra in excess of those associated with the decays of the standard W and Z bosons. Limits can therefore be deduced on the production and decay of heavy W-like (W') and Z-like (Z') bosons. We obtain preliminary limits (95% C.L.) :

$$\sigma_{W'} \cdot B_{e\nu} \leq 7.6 \text{ pb}$$

$$\sigma_{Z'} \cdot B_{e^+e^-} \leq 1 \text{ pb.}$$

These limits can be used to obtain mass limits on the W' and Z' bosons provided we specify their couplings. If the heavy bosons have the same weak charge as the standard model W and Z, and the same leptonic branching ratios, then the corresponding mass limits (95% C.L.) are :

$$m_W \geq 380 \text{ GeV}/c^2$$

$$m_Z \geq 400 \text{ GeV}/c^2.$$

3.5 The Number of Light Neutrino Types

The ratio $R \equiv (\sigma_W \cdot B_{e\nu}) / (\sigma_Z \cdot B_{e^+e^-})$ has been measured by CDF to be $R = 10.3 \pm 0.8 \pm 0.5$ (preliminary), and $R \leq 11.4$ (90% C.L.). The statistical error on R (± 0.8) arises predominantly from the limited Z statistics. Since the predicted W branching ratio is sensitive to the partial width for the decay $W \rightarrow tb$ and the predicted Z branching ratio is sensitive to the number of $Z \rightarrow \nu\nu$ channels open, the predicted value of R is sensitive to both the top quark mass (m_t) and the number of light neutrino types (N_ν). The measured value of R is compared with the predictions as a function of N_ν and m_t in fig. 13. We conclude that for a heavy top quark ($m_t \geq 80 \text{ GeV}/c^2$) there are either 3 or 4 light neutrino types.

3.6 W Plus Jets

High transverse momentum W bosons are expected and observed [9] to be produced in association with one or more hadronic jets arising predominantly from gluon bremsstrahlung off the incoming interacting partons. The measured rate of $W+1$ jet, $W+2$ jets, and $W+3$ jets in CDF agrees well with $O(\alpha_s^3)$ tree-level QCD calculations (fig. 14). Note that there is a theoretical uncertainty of $\pm 30\%$ on the $W+1$ jet prediction and $\pm 50\%$ on the $W+2$ jet prediction due to uncertainties on α_s and the Q^2 -scale. A preliminary analysis of the properties of the $W + \text{jet}(s)$ events also shows good agreement with QCD expectations based on the Papageno Monte Carlo and a full simulation of the CDF detector. In the following preliminary jet energy corrections have been applied. There are $\pm 10\%$ uncertainties remaining on the energy scale. Figs. 15a and 15b show that the P_T^W distributions for the $W+1$ jet and $W+2$ jet samples are well described by the QCD expectations, and fig. 15c shows good agreement between the measured and expected jet P_T distributions for $W+1$ jet events. For events with electron $E_T > 20 \text{ GeV}$, $\Delta E_T > 20 \text{ GeV}$, and $m_T^{e\nu} > 40 \text{ GeV}/c^2$ figs. 15d and 15e show the agreement between the expected and measured $m_T^{e\nu}$ distributions for $W+1$ jet and $W+2$ jet events, where jets with $E_T > 10 \text{ GeV}$ and $|\eta| < 2$ are counted. Finally fig. 15f shows that the two-jet mass distribution for $W+2$ jet events is also well described by QCD expectations.

4. Search for Supersymmetry

In supersymmetric models in which the SUSY quantum number is conserved the lightest supersymmetric particle is stable. If this particle is also neutral it will escape the interaction region undetected, giving rise to events in which there is a large ΔE_T . The other supersymmetric particles produced (e.g. squarks and gluinos) will decay to lighter supersymmetric particles, and normal quarks and gluons. Thus the final event will contain high- P_T jets associated with a large ΔE_T .

A preliminary search for supersymmetric particles in CDF has been performed on the 1988/9 data (4.6 pb^{-1}). Events have been selected with a large significant ΔE_T ($\Delta E_T > 40 \text{ GeV}$, $\Delta E_T / \sqrt{E_T} > 2.8$). To remove two-jet fluctuations, events with a jet ($E_T > 5 \text{ GeV}$) coplanar ($\pm 30^\circ$) to the ΔE_T vector have been rejected. Events with at least two calorimeter clusters ($E_T > 15 \text{ GeV}$, $|\eta| < 3.5$) were then retained for further analysis if the clusters had an EM fraction between 0.1 and 0.9, and if at least one cluster was central ($|\eta| < 1$). To remove W and Z decays, events with a cluster ($E_T > 15 \text{ GeV}$) with EM fraction > 0.9 , or with a high- P_T muon candidate ($P_T > 15 \text{ GeV}/c$) were rejected. Pathological events (noise, cosmics, readout problems, beam-gas interactions) were rejected by scanning.

Table 2 : Expected number of events in large-missing- E_T data sample from standard model processes compared to the observed number of events.

EXPECT	$\Delta E_T > 40 \text{ GeV}$	$\Delta E_T > 60 \text{ GeV}$
W, Z Decays	116 ± 30	24 ± 15
Heavy Quarks	42 ± 42	14 ± 14
TOTAL	158	38
OBSERVE	184	34

The ΔE_T distribution for the 184 events that survive the cuts is shown in fig. 16. The expected event rate from standard model processes is tabulated in table 2. The standard model expectations account for the observed event rate. There is no evidence for an excess of events ascribable to supersymmetric processes. To obtain a limit on the squark mass we assume that the photino is the lightest supersymmetric particle and is massless, and that

there are six degenerate squarks. The supersymmetric event rate and characteristics can then be predicted as a function of the squark and gluino masses. We obtain

$$m_{\tilde{q}} > 140 \text{ GeV}/c^2 \text{ (90\% C.L.)}$$

for all gluino masses. To obtain this preliminary result no standard model background subtraction has been made. Further work is in progress to obtain the corresponding gluino mass limit.

5. Search for the Top Quark

The dominant top quark production mechanism at the Tevatron collider is expected to be via the process $gg \rightarrow t\bar{t}$ (fig. 17). The purely hadronic final states for the top quark decay are swamped by QCD light quark multijet backgrounds. In the CDF analysis a search has therefore been made for semileptonic top quark decays. This search is sensitive provided the top quark decays predominantly via the charged weak current as expected in the standard model. Searches in two final states have been made: (i) electron plus ΔE_T plus ≥ 2 jets, and (ii) electron plus muon.

5.1 Electron + ΔE_T + ≥ 2 Jets

The measured inclusive electron P_T distribution is well described [10] in terms of $b\bar{b}$ production and semileptonic decay (which dominates in the region $P_T < 20 \text{ GeV}/c$) and W/Z decay (which dominates in the region $P_T > 20 \text{ GeV}/c$). To search for top decays, events with central electrons have been selected ($|\eta| < 1$, good fiducial region, good transverse shower shape, EM fraction > 0.5 , $0.5 < E/P < 1.4$, good track-strip chamber match, good isolation, remove photon conversions). Events with ≥ 2 jets ($E_T > 10 \text{ GeV}$, $|\eta| < 2.2$) have been retained for further analysis. Two data samples have then been extracted : (1) High-mass top quark sample; requiring electron $E_T > 20 \text{ GeV}$ and $\Delta E_T > 20 \text{ GeV}$, and (2) Low-mass top quark sample; requiring electron $E_T > 15 \text{ GeV}$, $\Delta E_T > 15 \text{ GeV}$, and (electron $E_T + \Delta E_T$) $> 40 \text{ GeV}$. The electron -"neutrino" transverse mass distributions for the two data samples are consistent with expectations for $W \rightarrow e\nu$ decay (fig. 18), and show no evidence for a contribution from the decay of a heavy top quark. The resulting top cross-section limit is shown as a function of m_t in fig. 19a. Comparing this with theoretical expectations for $t\bar{t}$ production at the collider we conclude that

$$40 < m_t < 77 \text{ GeV}/c^2 \text{ is excluded (95\% C.L.)}$$

5.2 Electron plus Muon

A search for high- P_T central electrons ($E_T > 15$ GeV, $|\eta| < 1$) produced in association with a high P_T central muon ($P_T > 45$ GeV/c, $|\eta| < 1.2$) has been made in 4.4 pb⁻¹ of 1988/9 data. One event passes these cuts. We expect 0.7 events to satisfy the cuts from standard model processes ($Z \rightarrow \tau^+\tau^-$ [0.5 events], W^+W^- [0.15 events], WZ [0.05 events]). However, to be conservative, we compute upper limits on the $t\bar{t}$ production cross-section (fig. 19b) as a function of m_t based on the observation of one event (no background subtraction). Comparing this limit with theoretical expectations for $t\bar{t}$ production we conclude that

$$30 < m_t < 72 \text{ GeV}/c^2 \text{ is excluded (95\% C.L.).}$$

We note that in the region of lower electron and muon transverse momenta we observe many events with kinematic characteristics in broad agreement with our expectations for $b\bar{b}$ production and semileptonic decay. Further details of the top quark searches in CDF can be found in ref. [10].

6. Search for a Light Higgs Boson

A search for a light Higgs Boson ($200 \text{ MeV}/c^2 < m_H < 1.5 \text{ GeV}/c^2$) produced in association with W or Z Bosons (fig. 20) is in progress in CDF. The method is similar to that described in ref. [11]. The predicted fraction of W and Z events containing an associated Higgs Boson is shown as a function of m_H in fig. 21. A light Higgs Boson is produced in about 1% of all W and Z events. Higgs Bosons with mass above the e^+e^- threshold and below the $\rho^+\rho^-$ threshold will decay predominantly to a charged track pair (e^+e^- , $\mu^+\mu^-$, $\pi^+\pi^-$ or K^+K^-). The predicted branching fractions are shown as a function of m_H in fig. 22. The predicted lifetime of the Higgs Boson increases rapidly below the $\mu^+\mu^-$ threshold. Above the $\mu^+\mu^-$ threshold the lifetime is short and the charged track pair will be associated to the vertex (fig. 23). The Higgs Boson is expected to be produced at relatively high transverse momentum (p_T), resulting in a high- p_T charged track pair (fig. 24). The signature for a light Higgs Boson produced in association with a W or Z Boson is therefore an isolated high- p_T charged track pair.

Preliminary results from a search for isolated high- P_T track pairs in W and Z events indicate that there is a substantial background from fluctuations of initial state bremsstrahlung jets produced in association with the weak boson. Never-the-less when the

analysis is complete it is expected that the search will have sufficient sensitivity to find or exclude a Higgs Boson with mass between the $\mu^+\mu^-$ and K^+K^- thresholds.

7. Conclusions

Results from the 1987 CDF run and preliminary results from the 1988/9 run indicate that the Standard Model gives an excellent description of the observed phenomenology of hard proton-antiproton interactions (the physics of jets, W, Z, heavy flavors, and missing E_T) at $\sqrt{s} = 1.8$ TeV. There is no direct evidence as yet for the top quark, or for fourth generation quarks or leptons, quark substructure, heavy W-like or Z-like bosons, or supersymmetric particles. In the coming months further analysis of the recent data will improve the sensitivity of the searches for deviations from standard model expectations and yield precision measurements of standard model physics.

References

- [1] F. Abe et al. (CDF Collab.) Nucl. Instr. and Meth. **A271**(1988)387.
- [2] J. Huth (CDF Collab.), Proc. of the SSC Workshop on Calorimetry for the SSC, Tuscaloosa, Alabama, March 1989; Fermilab-Conf-89/117-E.
- [3] D. Duke and J. Owens, Phys. Rev. **D27**(1984)508.
- [4] E. Eichten et al., Phys. Rev. Lett. **50**(1983)811.
- [5] G. Arnison et al. (UA1 Collab.) Nucl. Phys. **B276**(1986)253.
- [6] M. Althoff et al. (TASSO Collab.) Z. Phys. **C22**(1984)307.
- [7] F. Berends et al., Z. Phys. **C27**(1985)155; F. Berends and R. Kleiss, Z. Phys. **C27**(1985)365. Also used were calculations by B. Marchesini and B. Webber, Nucl. Phys. **B310**(1988)461; G. Bonvicini and L. Trentadue, UM-HE-88-36.
- [8] F. Abe et al. (CDF Collab.) Phys. Rev. Lett. **63**(1989)720.
- [9] S. Geer and W. J. Stirling, Phys. Lett. **152B**(1985)373.
- [10] F. Abe et al. (CDF Collab.), in preparation.
- [11] S. Geer, UA1 technical note UA1 TN 88-29(1988), unpublished.

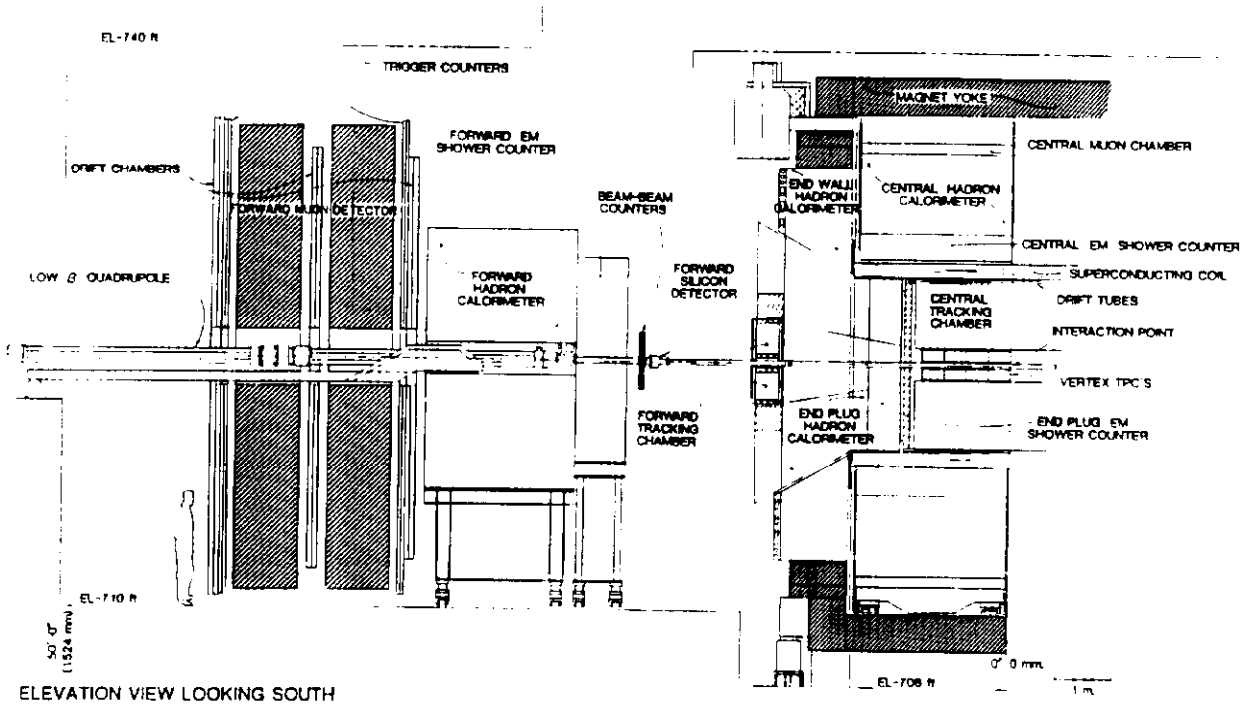


Fig. 1 : Cut-away view through the forward half of the CDF detector. The detector is forward-backward symmetric about the interaction point.

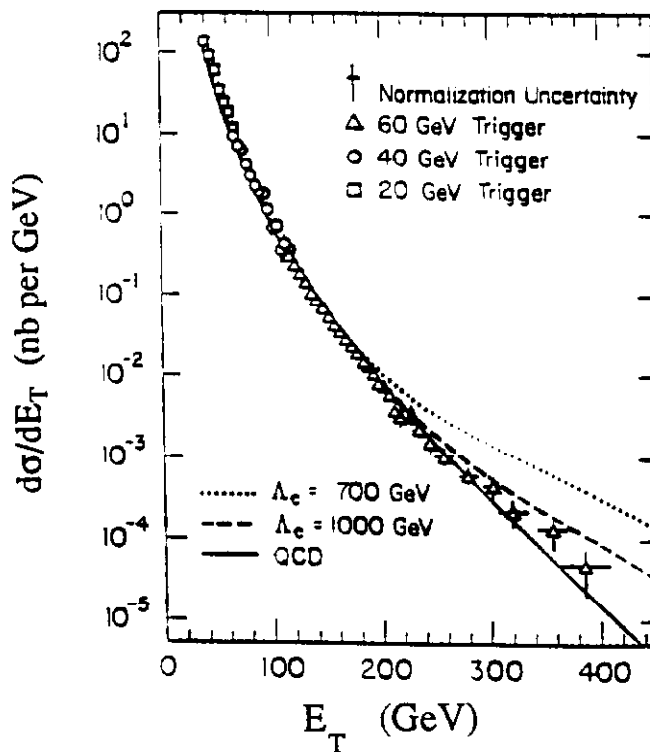


Fig. 2 : Inclusive differential jet cross-section. The curves show the leading order QCD expectation ($\Lambda_c = \infty$) using DO2 structure functions with $Q^2 = E_T^2/2$, and the expected modification which would arise from quark substructure [4] associated with the scale Λ_c .

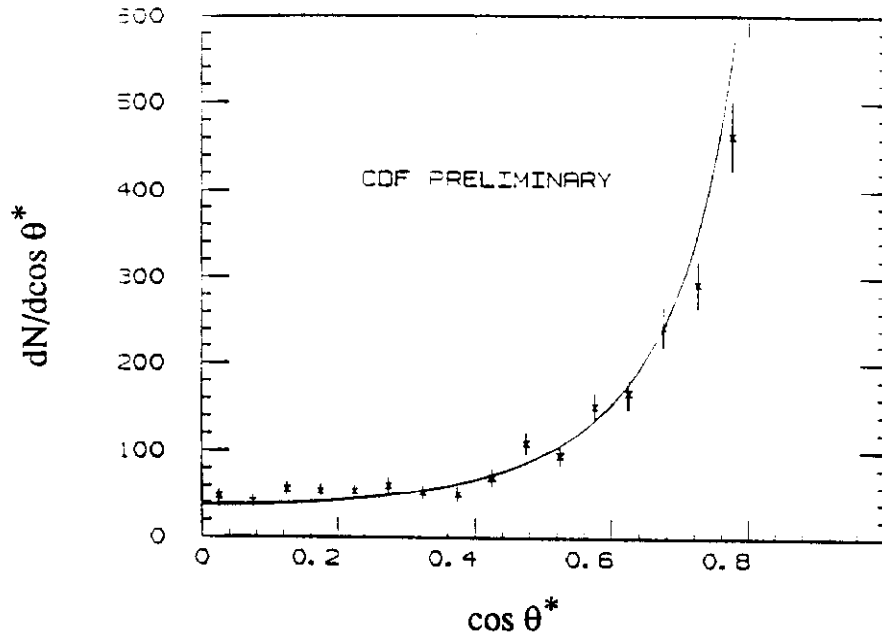


Fig. 3 : Uncorrected two-jet angular distribution ($m_{jj} > 300 \text{ GeV}/c^2$) compared with the leading order QCD prediction (curve).

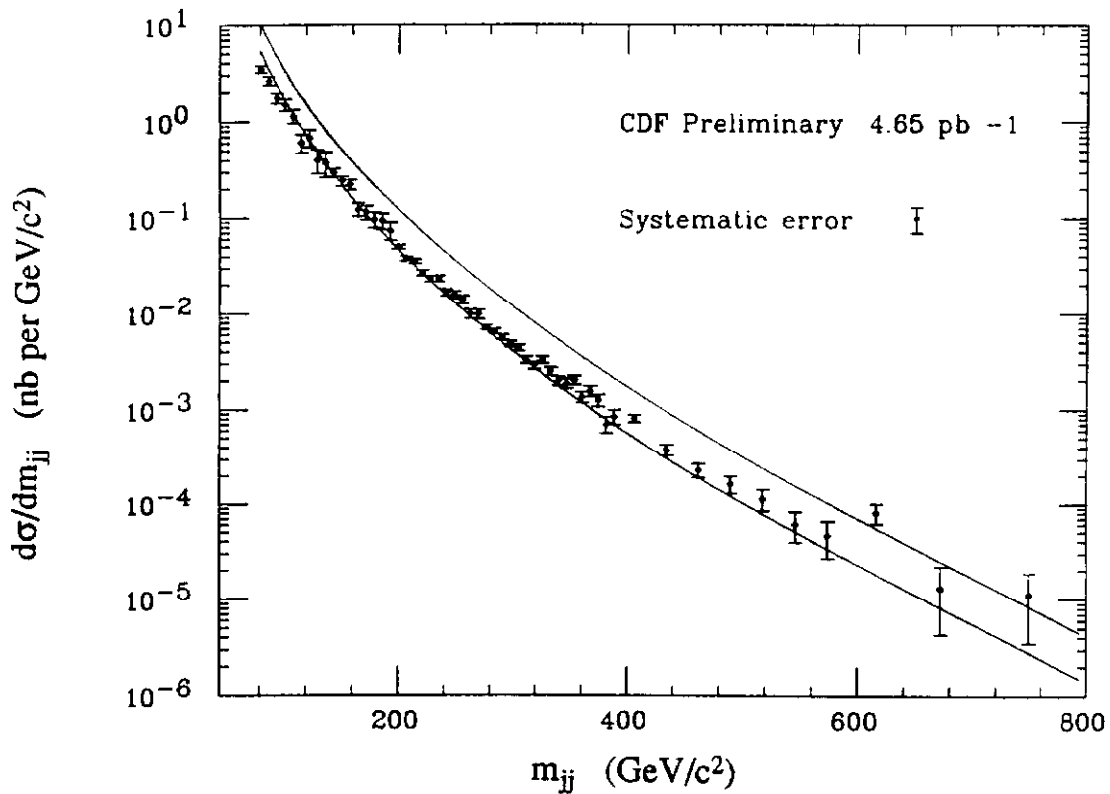


Fig. 4 : Two-jet mass distribution. The band shows the envelope of leading order QCD predictions which accommodates the GHR, DO1, DO2, and EHLQ1 structure functions.

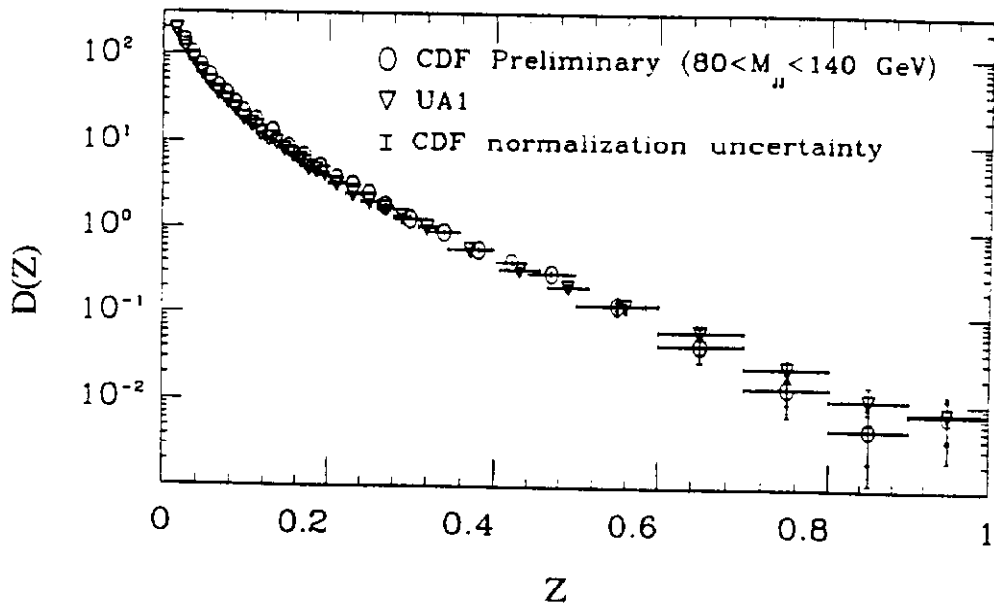


Fig. 5 : Jet fragmentation function. The preliminary CDF result is compared with the result from the UA1 experiment [5] for jets with $P_T > 25 \text{ GeV}/c$.

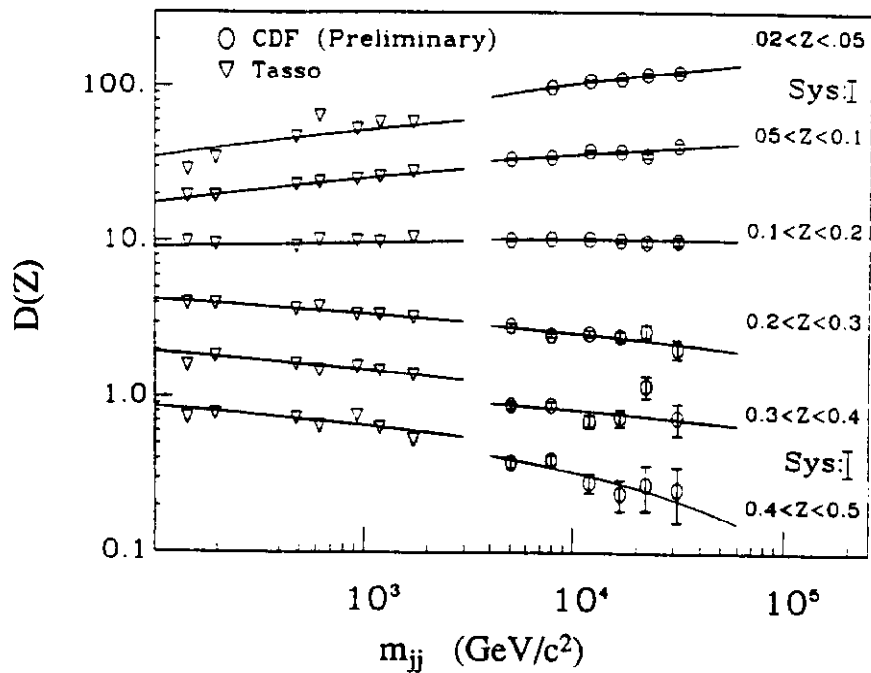


Fig. 6 : Dependence of jet fragmentation on the Q^2 -scale and the fragmentation variable z . Results from jets produced in e^+e^- annihilation measured by the TASSO experiment [6] are shown for comparison.

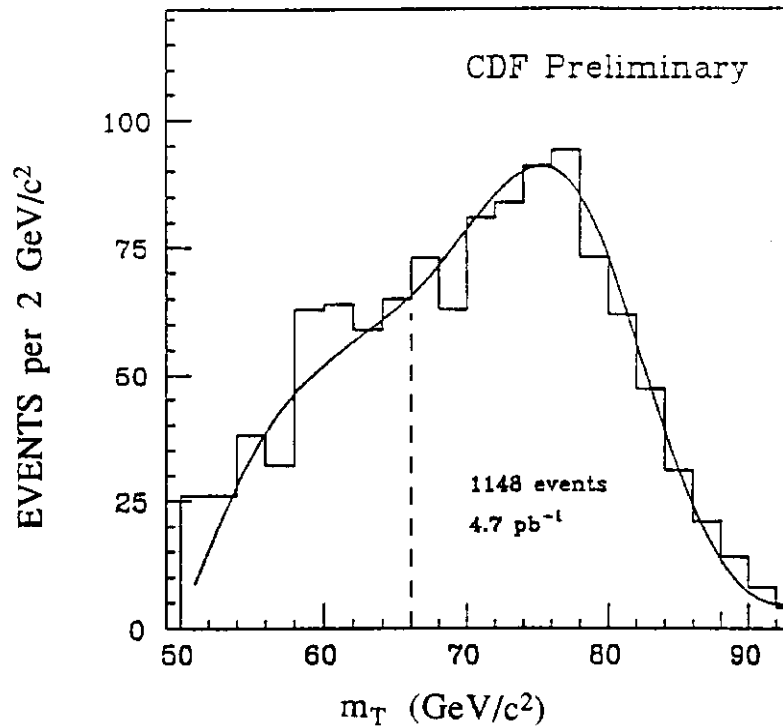


Fig. 7 : Electron-neutrino transverse mass distribution for $W \rightarrow e\nu$ candidates. The curve shows the best fit.

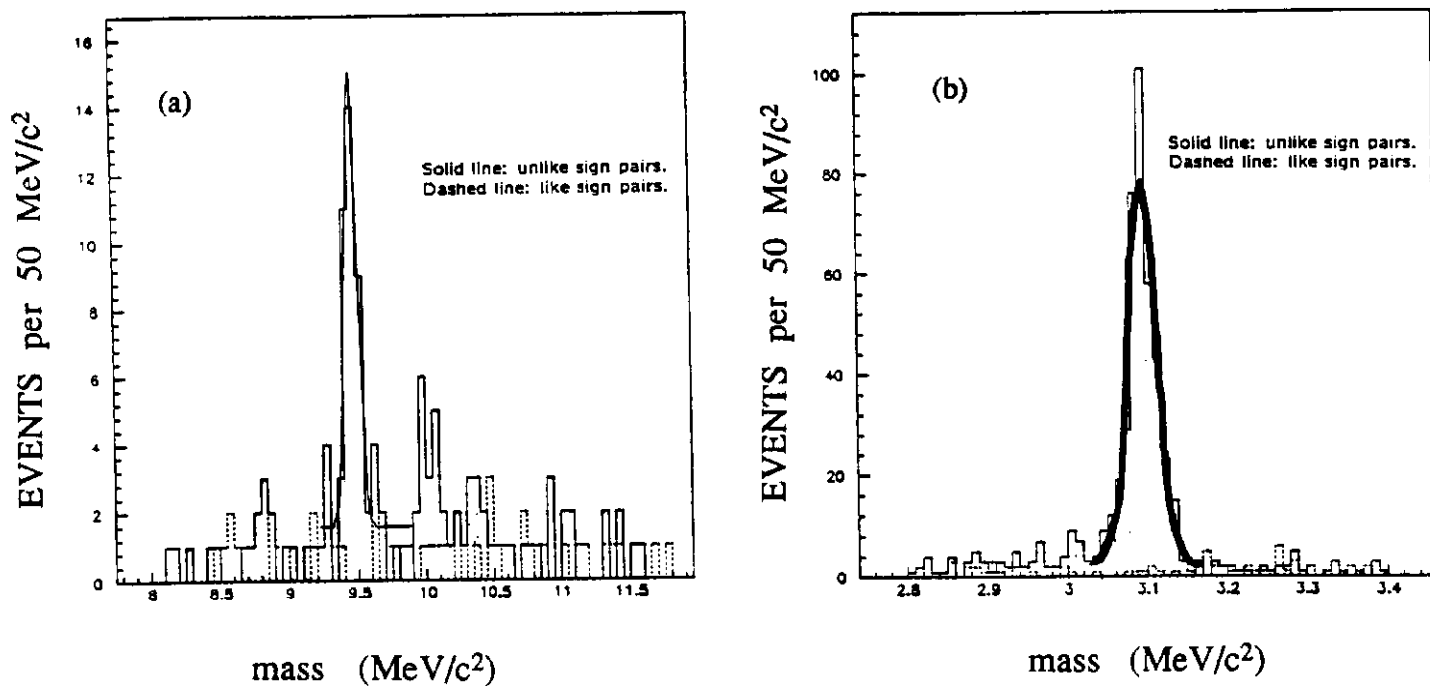


Fig. 8 : The $\mu^+\mu^-$ mass spectrum in the neighbourhood of (a) the Υ , and (b) the J/ψ resonances. The tracks have been constrained to come from the beam axis.

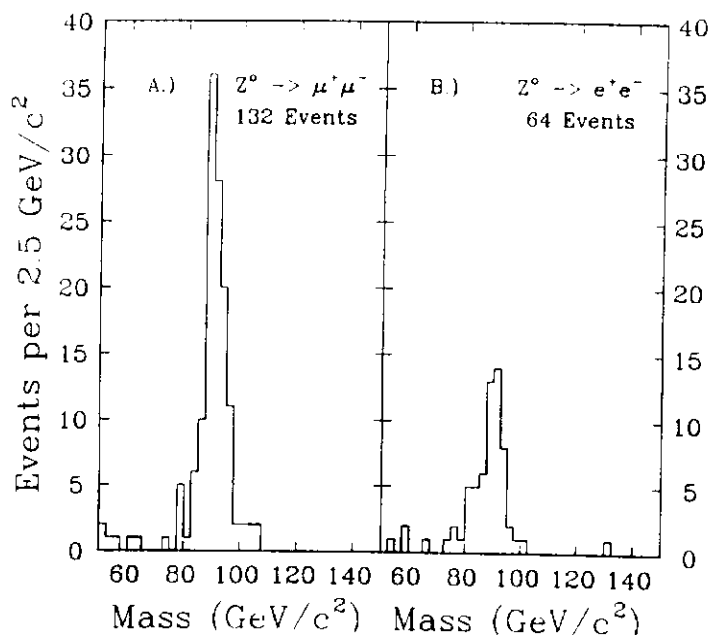


Fig. 9 : Mass distribution for (a) $Z \rightarrow \mu^+\mu^-$ and (b) $Z \rightarrow e^+e^-$ candidates using tracking information.

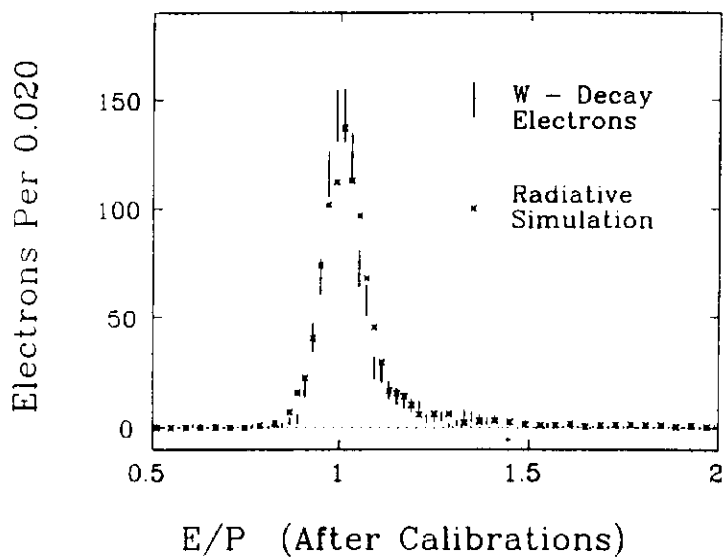


Fig. 10: Ratio of electromagnetic energy to track momentum for electrons in the W sample compared to a Monte Carlo prediction which includes radiative corrections and the CTC resolution.

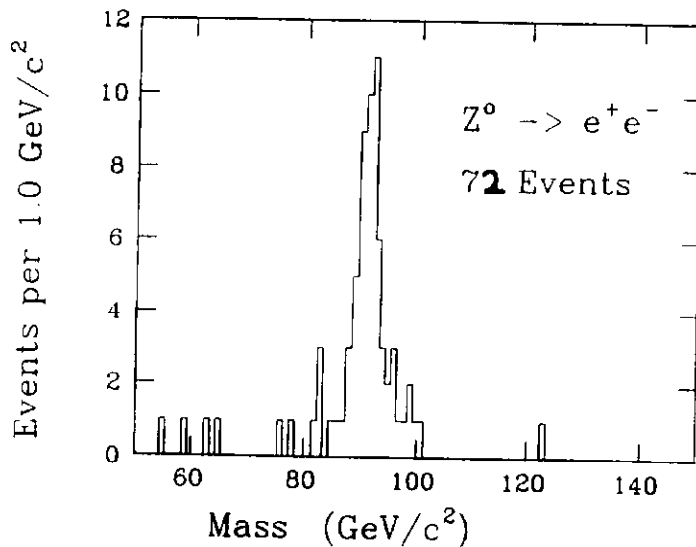


Fig. 11: Mass distribution for $Z \rightarrow e^+e^-$ candidates using calorimeter energies.

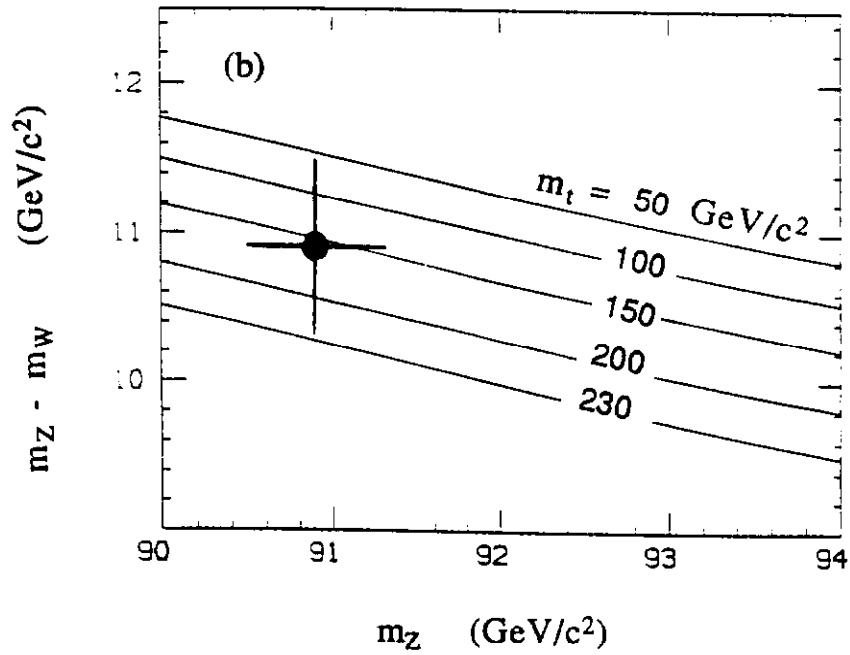
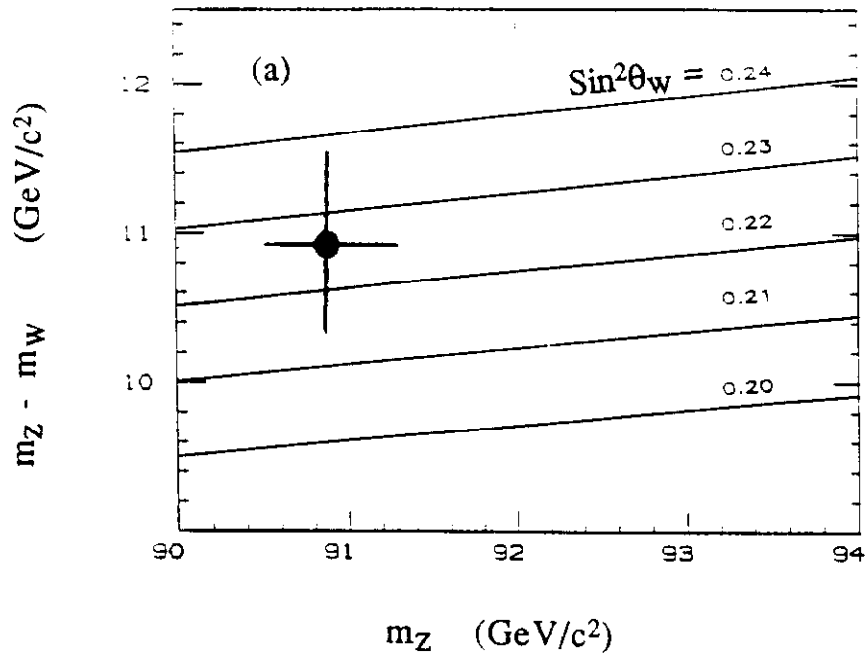


Fig. 12: The measured values of $(m_Z - m_W)$ and m_Z compared with Standard Model expectations as a function of (a) $\sin^2 \theta_W$, and (b) top quark mass (assuming $m_{\text{HIGGS}} = 100 \text{ GeV}/c^2$).

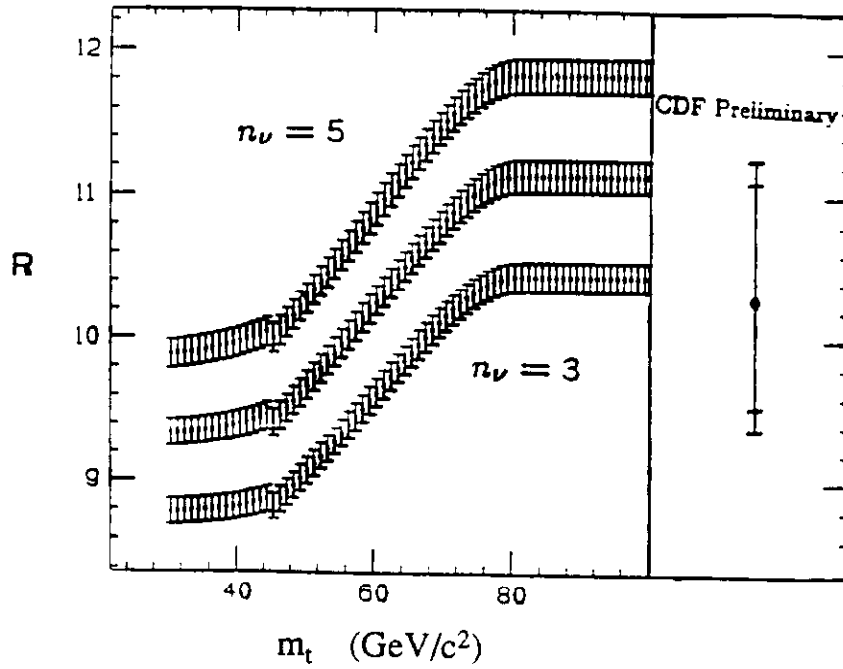


Fig. 13: The measured value of $R \equiv (\sigma_W \cdot B_{e\nu}) / (\sigma_Z \cdot B_{e^+e^-})$ compared with Standard Model expectations as a function of top quark mass. The bands show the predictions for 3, 4, and 5 neutrino types, and accommodate the MRS structure functions based on BCDMS data (MRSB) and EMC data (MRSE).

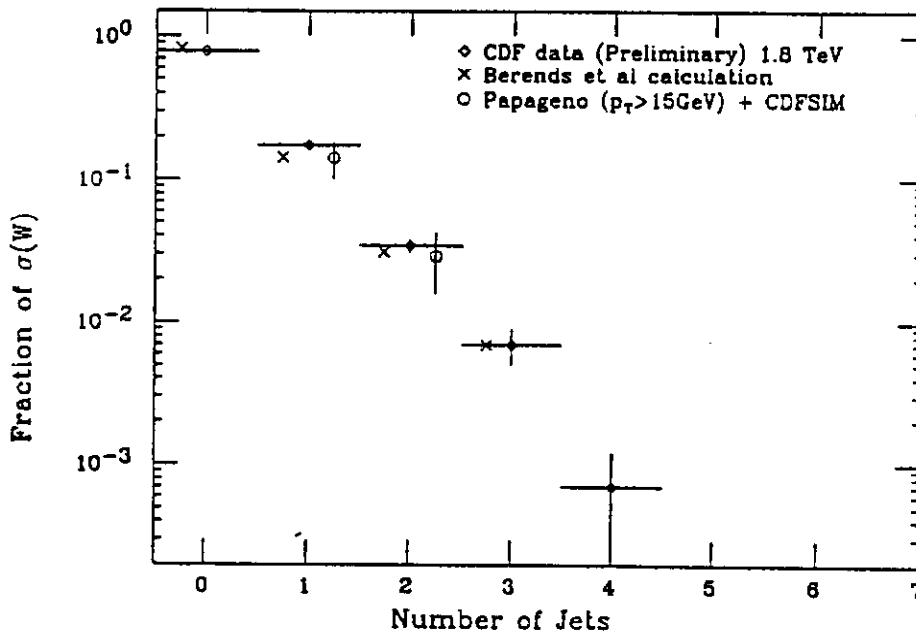


Fig. 14: Observed fraction of W events in which 0, 1, 2, 3, and 4 jets (uncorrected $E_T > 10$ GeV, $|\eta| < 2.2$) have been produced in association with the W. Measurements are compared with tree-level predictions.

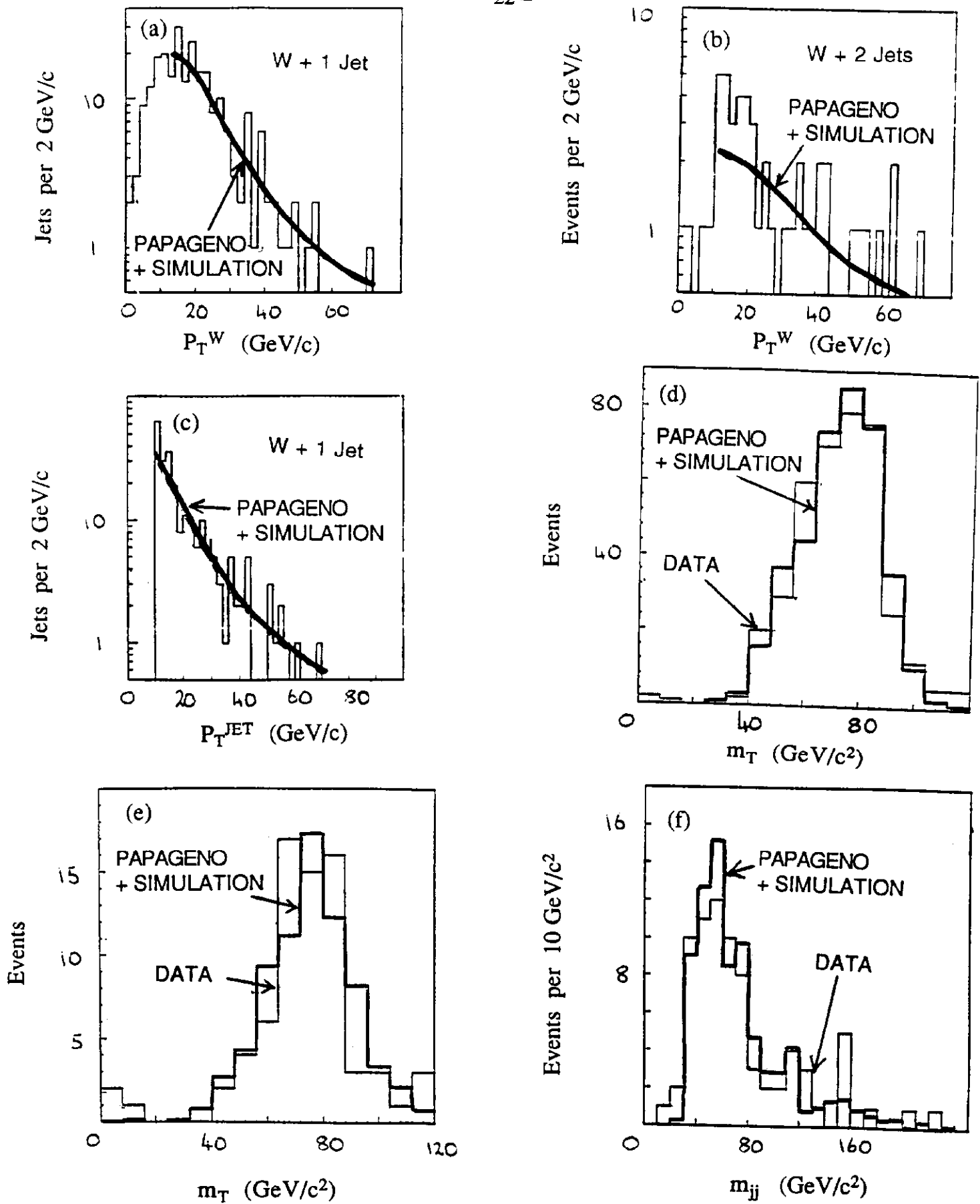


Fig. 15: Properties of W + jet(s) events (see text) compared with expectations based on the Papageno Monte Carlo.

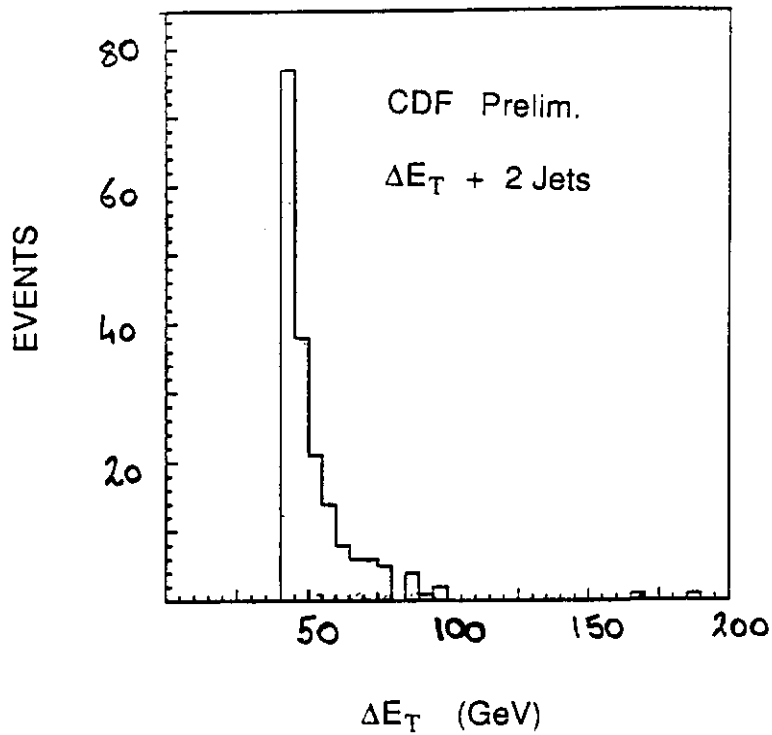


Fig. 16: Missing E_T distribution for events with two jets passing the selection described in the text.

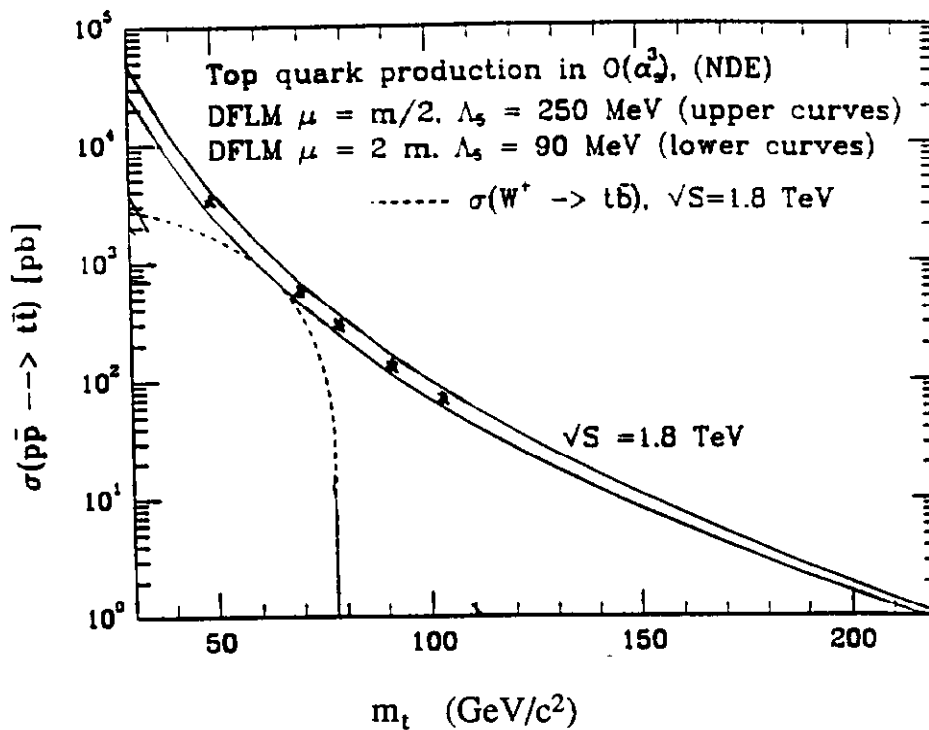


Fig. 17: Expected top quark production cross-section at the Tevatron Collider shown as a function of top quark mass. The contributions from strong and weak production are shown separately.

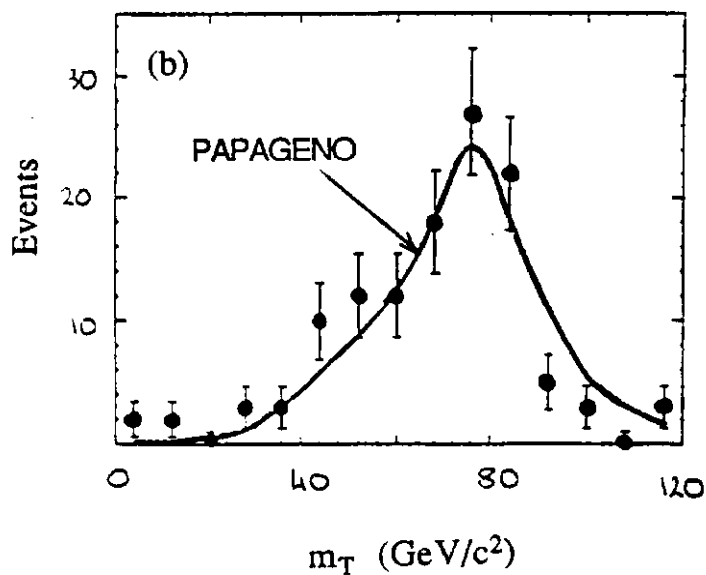
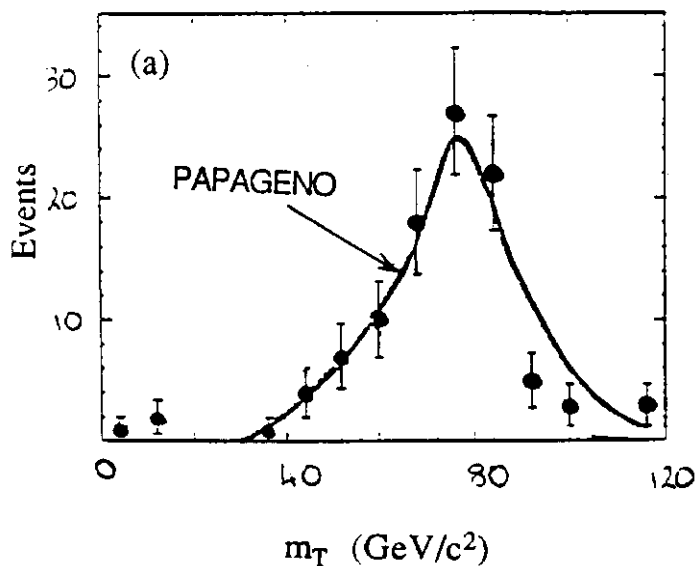


Fig. 18: Electron-neutrino transverse mass distributions for the (a) high-mass top quark sample, and (b) low-mass top quark sample (see text) compared with expectations (curve) for $W + 2$ jet production followed by $W \rightarrow e\nu$ decay.

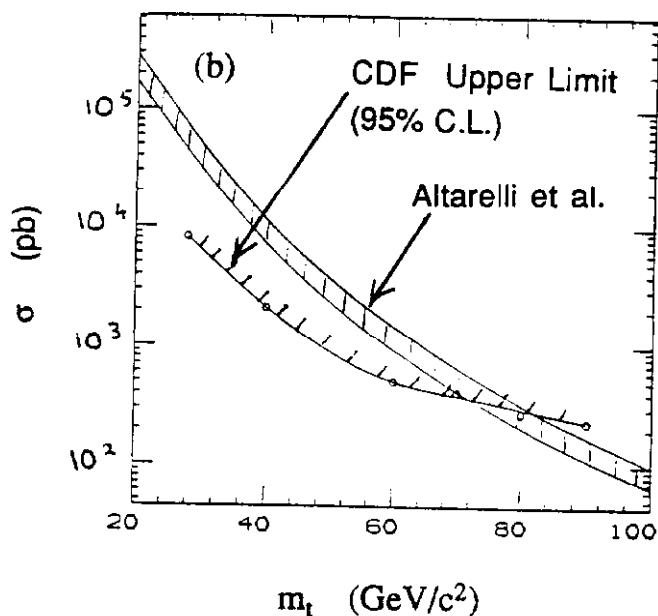
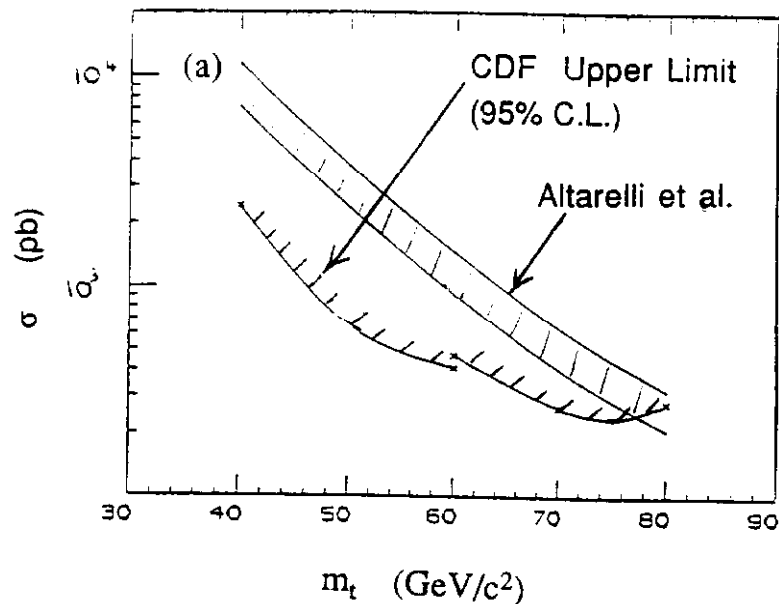


Fig. 19: Upper limits on the top quark production cross-section shown as a function of top quark mass, from (a) the electron + $\Delta E_T \geq 2$ jets search, and (b) the electron + muon search. The theoretical expectation is also shown. The band reflects structure function and Q^2 -scale uncertainties.

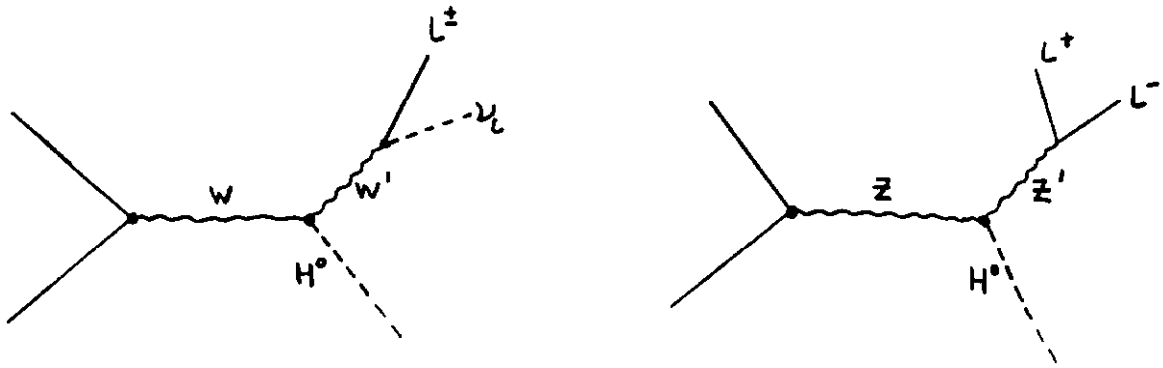


Fig. 20: Higgs production in association with W and Z bosons.

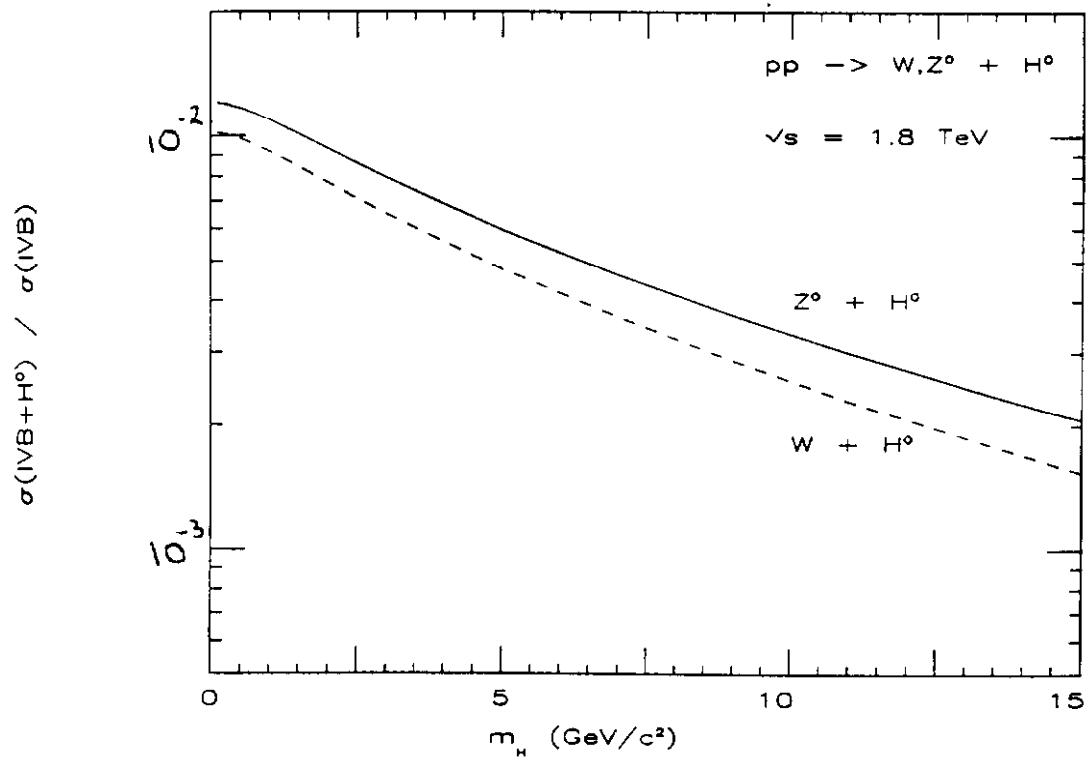


Fig. 21: Predicted fraction of W and Z bosons produced in association with a Higgs boson at the Tevatron Collider shown as a function of Higgs boson mass.

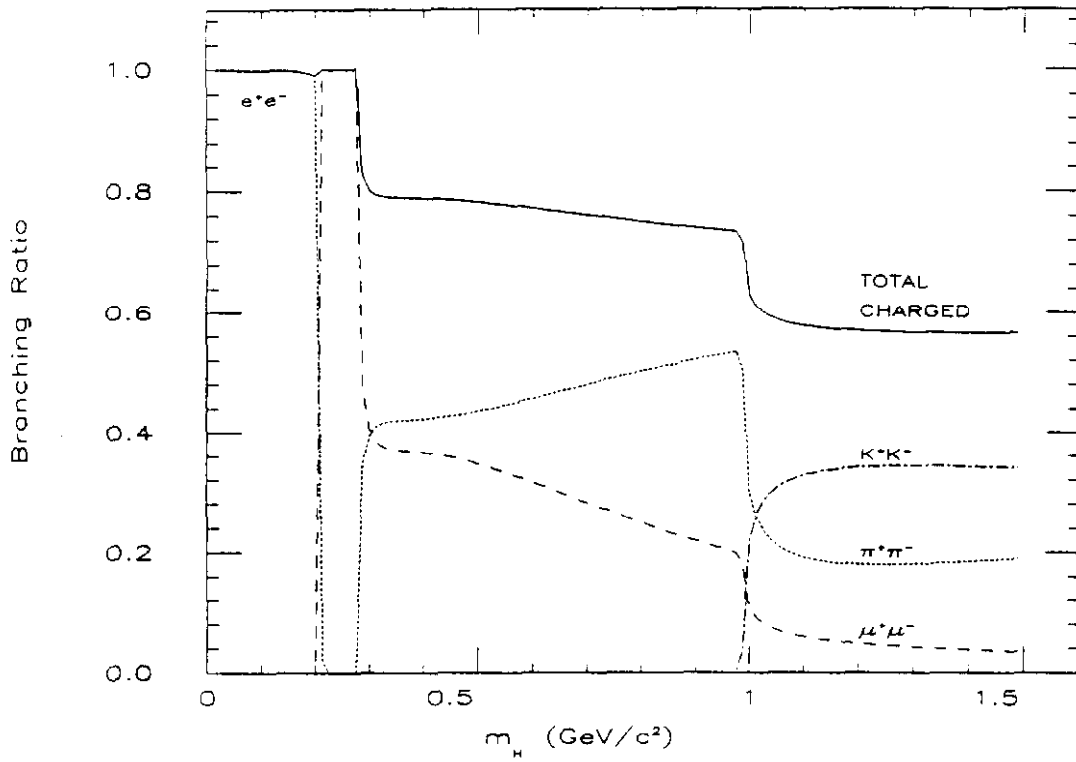


Fig. 22: Higgs boson decay branching ratios shown as a function of Higgs boson mass.

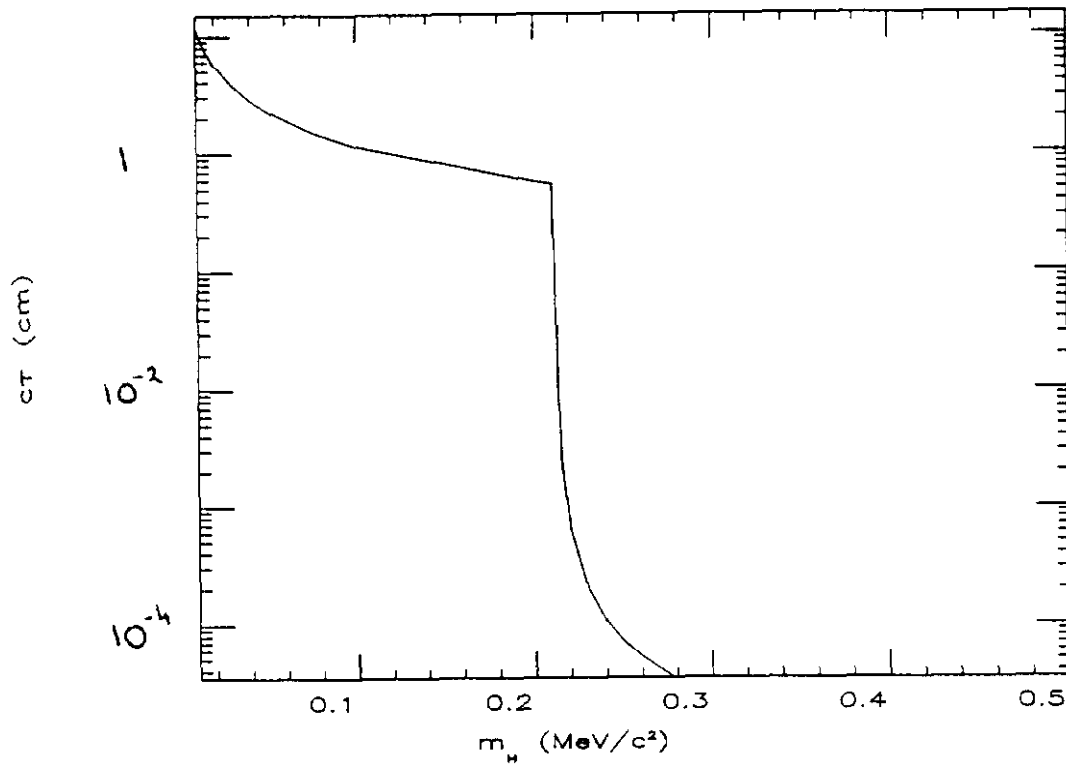


Fig. 23: Higgs boson decay length $c\tau$ shown as a function of Higgs boson mass.

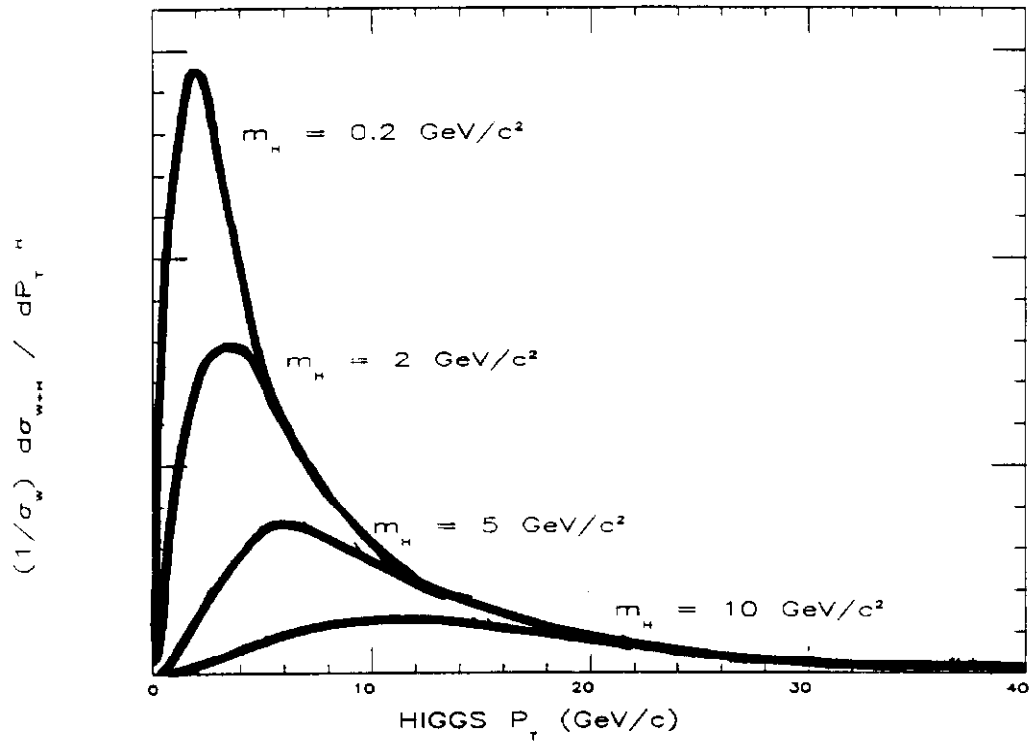


Fig. 24: Expected transverse momentum spectrum for Higgs bosons produced in association with W bosons (fig. 20) at the Tevatron Collider shown for several Higgs boson masses.